ACS OMEGA

http://pubs.acs.org/journal/acsodf

Article

3-Pyridylacetic-Based Lanthanide Complexes Exhibiting Magnetic Entropy Changes, Single-Molecule Magnet, and Fluorescence

Ying-Bing Lu,* Jun-Wei Wu, Shui-Dong Zhu,* Sheng-Qian Wang, Shi-Yong Zhang, Cai-Ming Liu,* Rong Li, Juan Li, Jia-Hao Ai, and Yong-Rong Xie

Cite This: *ACS Omega* 2022, 7, 2604−2612

Read Online

ACCESS | Metrics & More | Article Recommendations | Supporting Information

ABSTRACT: Four complexes from lanthanides, 3-pyridylacetate, and 1,10-phenanthroline, formulated as $[Ln_2(3\text{-PAA})_2(\mu\text{-Cl})_2(phen)_4](ClO_4)_2$ [Ln = Gd(**1**), Dy(**2**), Eu(**3**), Tb(**4**), 3-PAA = 3-pyridylacetic acid, phen = 1,10-phenanthroline], were obtained. The four compounds were characterized by IR spectra, thermogravimetric analyses, powder X-ray diffraction, and single-crystal X-ray diffraction. Compounds **1**−**4** are isomorphous, and they have a dinuclear structure. Magnetic studies reveal that **1** shows the magnetocaloric effect with $-\Delta S_m^{max}$ = 19.03 J kg^{-1} K^{-1} at 2 K for ΔH = 5 T, and **2** displays a field-induced single-molecule magnet with U_{eff} = 19.02 K. The photoluminescent spectra of **3** and **4** exhibit strong characteristic emission, which demonstrate that the ligand-to-Eu^{III}/Tb^{III} energy transfer is efficient.

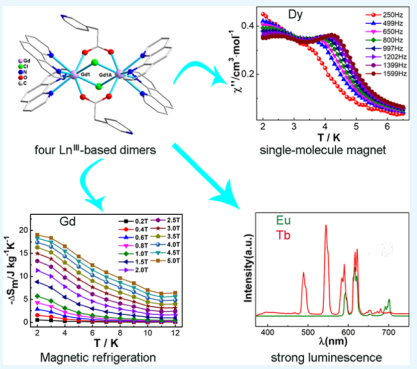

INTRODUCTION

Lanthanide-based complexes have received considerable interest because of their remarkable properties stemming from unique 4f electrons of lanthanide ions.[1−4] On the one hand, Ln-based complexes hold a prominent position in magnetism.[5,6] For example, Gd(III) ion with a large spin ground state S, D_{ion} = 0, and low-lying excited spin states is considered as a potential candidate for molecular refrigerant materials with a large magnetocaloric effect (MCE).[7,8] Such materials are sought because of their potential applications in cryogenic refrigeration.[9−11] Dy(III) ion with large magnetic moment and strong anisotropy is regarded as an ideal spin carrier for single-molecule magnets (SMMs),[12−14] which is the major breakthrough in the field of magnetic research in the recent two decades. Such magnets are favored because of their similar memory effects observed in magnetic nanoparticles and their potential application in high-density data storage quantum computing and spintronics of molecular dimensions.[15] To date, great progress has been made in Dy(III)-based SMMs, such as mononuclear and polynuclear Dy^{III} systems.[16−20] For example, Tong and Mills' groups reported two Dy(III)-SMMs showing hysteresis at a liquid nitrogen temperature.[21,22] The anisotropy of Dy^{III} primarily originates from the unquenched orbital momentum of the ion, but it is also affected by the ligand field.[23] Therefore, the design and synthesis of SMMs remain a challenge, and ligands are important for the preparation of Ln-based SMM. In addition, previous achievements demonstrate that intramolecular magnetic exchange can decrease tunnel splitting (T), which can effectively suppress quantum tunneling of magnetization (QTM) and then greatly improve the effective barrier (U_{eff}).[24] Hence, the design and construction of the simplest polynuclear SMM, a Dy_2 system, are important because such species can offer a good platform for a comprehensive understanding of magnetic exchange and the origin of magnetism in SMMs.

On the other hand, luminescence from lanthanides has aroused considerable attention because of their outstanding optical properties such as long-lived emissions, high quantum yields, narrow bandwidth, and large Stokes shifts, as well as their wide applications in lasers, sensing, white-light emission, luminescent thermometers, and color displays.[25−27] Among lanthanide ions, Eu^{III} and Tb^{III} are considered important optical centers because of their strong, visible, and easily detected emissions. However, the direct excitation of lanthanide ions is disfavored because of their spin- and parity-inhibited f−f transitions.[28,29] One effective method is to introduce suitable π-conjugated ligands, which can absorb light and transfer energy to Ln^{III} ions (antenna effect), thereby improving lanthanide luminescence.[30,31] Hence, organic ligands play a key role in the construction of luminescent Ln complexes.

In addition, pyridylecarboxylic ligands are a class of attractive ligands bearing N and O coordination atoms,

Received: August 29, 2021
Accepted: November 30, 2021
Published: January 11, 2022

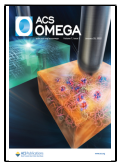

https://doi.org/10.1021/acsomega.1c04728
ACS Omega 2022, 7, 2604−2612

which have been extensively used to construct complexes showing structural variations and excellent properties because of their exceptional coordination ability and various coordinating modes.[32] However, the 3-pyridylacetic ligand (3-PAA) as an important and simple pyridylecarboxylic ligand has received less attention. Based on previous reports, no example of 3-pyridylacetate-based Ln complexes has been reported, and only several transition-metal complexes with 3-PAA have been reported.[33−36] As a part of our continuous studies on Ln complexes with magnetic and luminescent properties,[37,38] herein, a series of Ln-based complexes are obtained using 3-PAA and 1,10-phenanthroline (phen) as auxiliary ligands. This work is based on the following ideas: (1) Ln-based complexes fabricated by 3-PAA are unexplored, which provide substantial research opportunities; (2) phen as a kind of *N*,*N*′ bulky auxiliary ligands can block the high coordination sites of lanthanide centers, which can achieve polynuclear Ln-based SMMs with isolated structures; and (3) the 3-PAA and phen ligands are aromatic π-conjugated molecules, which can serve as chromophoric antenna ligands to sensitize lanthanide luminescence. In this work, four new Ln-based complexes, namely, $[Ln_2(3\text{-PAA})_4(\mu\text{-Cl})_2(phen)_4]$ [Ln = Gd(**1**), Dy(**2**), Eu(**3**), Tb(**4**), 3-PAA = 3-pyridylacetic, and phen = 1,10-phenanthroline], were prepared, and they show a dinuclear structure. **1** shows the MCE with $-\Delta S_m^{max}$ = 19.03 J kg^{-1} K^{-1} at 2 K for ΔH = 5 T, whereas **2** exhibits SMM behavior. The photoluminescent properties of **3** and **4** have also been investigated. Notably, the four complexes represent the first lanthanide-based complexes constructed from 3-PAA.

RESULTS AND DISCUSSION

Synthetic Aspects. Multiple factors such as the concentration and type of reactants, pH value, reaction temperature, reaction time, and type of solvent can affect the formation and crystallization of final products in a solvothermal system. We obtained a family of novel Ln-based complexes by solvothermal reactions of the corresponding $Ln(ClO_4)_3\cdot 6H_2O$, 3-PAA·HCl, 1,10-phenanthroline, and Et_3N in CH_3CN. A series of systematic studies indicated that the pH and the temperature of the reaction play a key role for the resulting products. The initial pH values of the syntheses for **1**−**4** were in a range of 5.5−6.5. In addition, parallel experiments showed that the temperature of the reaction suitable products cannot be produced at 140, 160, and 180 °C (Scheme 1).

Scheme 1. Synthetic Procedure of Complexes 1−4

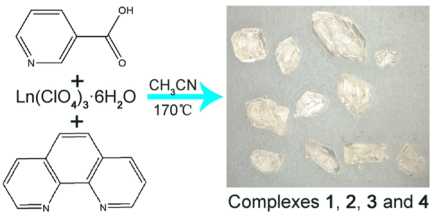

Structural Description and Discussion. Single-crystal X-ray diffraction analyses revealed that complexes **1**−**4** were isostructural, and such complexes crystallized in the monoclinic space group $P2_1/c$. PXRD studies showed that solid samples of the as-synthesized complexes **1**−**4** were in agreement with single-crystal X-ray diffraction studies, indicating the phase purity of **1**−**4** (Figure S1 in the Supporting Information (SI)). Pertinent crystal data and structure refinement results for **1**−**4** are summarized in Table 1, and selected bond lengths are listed in Table S1 in SI. All of the compounds were composed of cationic dimers $[Ln(PAA)(\mu\text{-Cl})(phen)_2]^{2+}$, which were charge-compensated perchlorate in the accessible voids. Herein, as an example, the structure of complex **1** was discussed in detail. As shown in Figure 1a, the asymmetric unit of **1** contains one crystallographically independent Gd^{III} ion, one PAA^{1-} ligand, one Cl^- anion, two phen molecules, and one ClO_4^- anion. The Gd^{III} center was eight-coordinated in an $O_2Cl_2N_4$ donor set, which was constructed by two carboxylate oxygen atoms from two different PAA^{1-} ligands, two Cl atoms, and four nitrogen atoms from two different chelated phen molecules. The polyhedral geometry of the Gd^{III} center was systematically analyzed using SHAPE 2.1 program.[39] The result showed that the coordination geometry of the Gd^{III} ion can be regarded as a distorted square antiprism (D_{4d} symmetry) with a continuous shape measurement (CShM) value of 1.381 (Figure 1b and Table S2 in the SI). The bond lengths of Gd−O were 2.349(2) and 2.352(2) Å; the bond length of Gd−Cl was 2.7759(7) Å, whereas the bond length of Gd−N ranged from 2.553(3) to 2.579(3) Å, which were close to those found in previously reported gadolinium−oxygen, chlorine, and nitrogen donor compounds.[40,41] As shown in Figure 1c, two neighboring Gd atoms were connected by two bridging Cl^- ions and two bridging carboxyl groups of two PAA^{1-} ligands to form a binuclear lanthanide cluster $[Gd_2(\mu\text{-Cl})_2(\mu\text{-OCOPAA})_2]^{2+}$, in which the Gd···Gd1A separation and Gd1−Cl1−Gd1A angle were 3.9059(3) Å and 89.747(21)°, respectively. In **1**, the PAA^{1-} ligand served as a bidentate ligand and adopted the μ_2−η^1:η^1 coordination mode to bind Gd^{III} ion by only using its carboxylate group, whereas its pyridine N atom was uncoordinated. This result was similar to other reported Ln complexes based on pyridylecarboxylic ligands. Then, these binuclear clusters were stacked together by face-to-face π−π stacking interactions from the phenyl rings of phen ligands, with a distance of 3.693(3) and 3.809(3) Å, generating a two-dimensional (2D) supramolecular layer along the *ab* plane (Figure 2), and counteranions $[ClO_4]^-$ were located in the accessible voids of these supramolecular layers along the *ab* plane (Figure S2 in the SI).

Thermal Behavior. As shown in Figure S3 in the SI, the thermogravimetric (TG) analysis (TGA) plots of complexes **1**−**4** showed that they had similar thermal behavior because they were isostructural, which is consistent with the reported isostructural complexes.[42] The thermogravimetric curve revealed that complexes **1**−**4** involved a loss of 34.50% (calcd 34.37%) for **1**, 34.72% (calcd 34.15%) for **2**, 34.55% (calcd 34.60%) for **3**, and 34.02% (calcd 34.22%) for **4** from 25 to 379 °C, which can be attributed to the release of two counteranions $[ClO_4]^-$ together with two Cl^- and the removal of two coordinated PAA^- ligand. And the subsequent pyrolysis process occurred from 379 to 800 °C due to the decomposition of the network. The result of the TG analysis basically agrees with that of the structure determination of **1**−**4**.

Magnetic Properties. In recent years, molecular cryomagnetic coolants have received considerable interest not only because they have potential applications in cryogenic refrigeration with high energy efficiency and environmental friendliness but also because they have a stoichiometric composition, modifiability, and monodispersity.[43−45] Previous

https://doi.org/10.1021/acsomega.1c04728
ACS Omega 2022, 7, 2604−2612

Table 1. X-ray Diffraction Crystallographic Data for 1−4

	Gd(1)	Dy(2)	Eu(3)	Tb(4)
formula	$C_{62}H_{44}Cl_4N_{10}O_{12}Gd_2$	$C_{62}H_{44}Cl_4N_{10}O_{12}Dy_2$	$C_{62}H_{44}Cl_4N_{10}O_{12}Eu_2$	$C_{54}H_{38}Cl_4N_{16}O_{12}Tb_2$
Fw	1577.37	1587.87	1566.79	1580.71
temp (K)	296(2)	296(2)	293(2)	296(2)
crystal system	monoclinic	monoclinic	monoclinic	monoclinic
space group	$P2_1/c$	$P2_1/c$	$P2_1/c$	$P2_1/c$
a (Å)	12.09360(10)	12.05930(10)	12.1286(12)	12.07650(10)
b (Å)	11.7499(2)	11.72510(10)	11.7919(11)	11.73330(10)
c (Å)	21.6432(3)	21.6822(2)	21.603(2)	21.6298(2)
β (deg)	92.6250(10)	92.7200(10)	92.461(3)	92.55
V (Å^3)	3072.24(7)	3062.33(5)	3086.8(5)	3061.85(5)
Z	2	2	2	2
D_c (g cm^{-3})	1.705	1.722	1.686	1.715
μ (mm^{-1})	2.385	2.667	2.257	2.537
F (000)	1556	1564	1552	1560
reflns collected	26 260	17 604	18 856	20 243
independent reflns	5498	5327	5215	5626
R_{int}	0.0235	0.0255	0.0236	0.0237
theta range (deg)	1.88−25.50	1.90−25.01	3.23−25.00	1.88−25.50
params/restraints/data	400/23/5498	400/829/5327	406/18/5215	400/18/5626
R_1 $[I > 2\sigma(I)]$[a]	0.0540	0.0424	0.0352	0.0407
wR_2 (all data)[b]	0.2463	0.1558	0.1308	0.1475
GOF on F^2	1.005	1.002	1.013	0.977
ρ_{max}/ρ_{min} (e Å^{-3})	0.7456/0.6682	0.7456/0.6592	1.000/0.784	0.7456/0.6372

[a] $R_1 = \sum||F_o| - |F_c||/\sum|F_o|$. [b] $wR_2 = [\sum w(F_o^2 - F_c^2)^2]/[\sum w(F_o^2)^2]^{1/2}$.

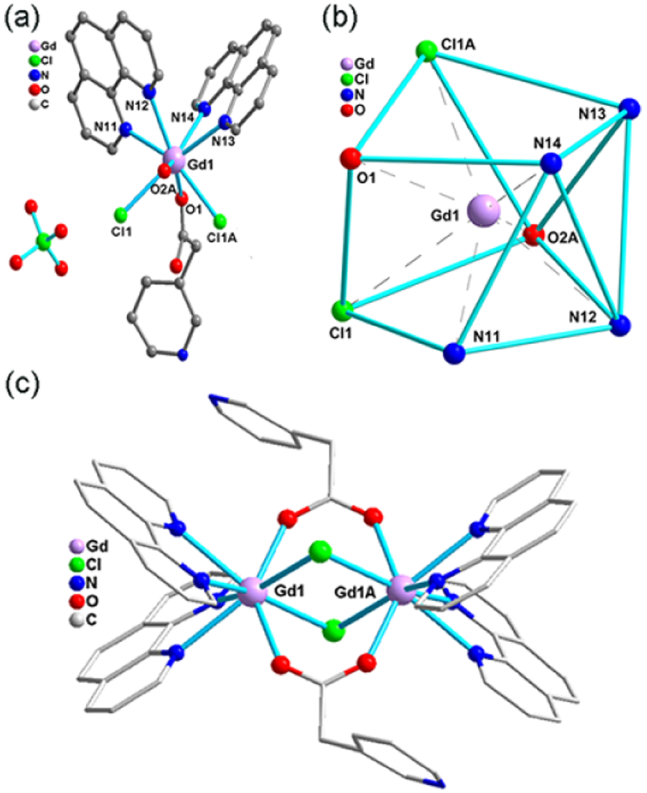

Figure 1. (a) Ball and stick plot showing the asymmetric unit of **1**. (b) Coordination polyhedron around the Gd^{III} ion in **1**. (c) Drawing of the dinuclear structure of **1**. H atoms and perchlorate are omitted for clarity. Symmetry code A: $1 - x$, $1 - y$, $-z$.

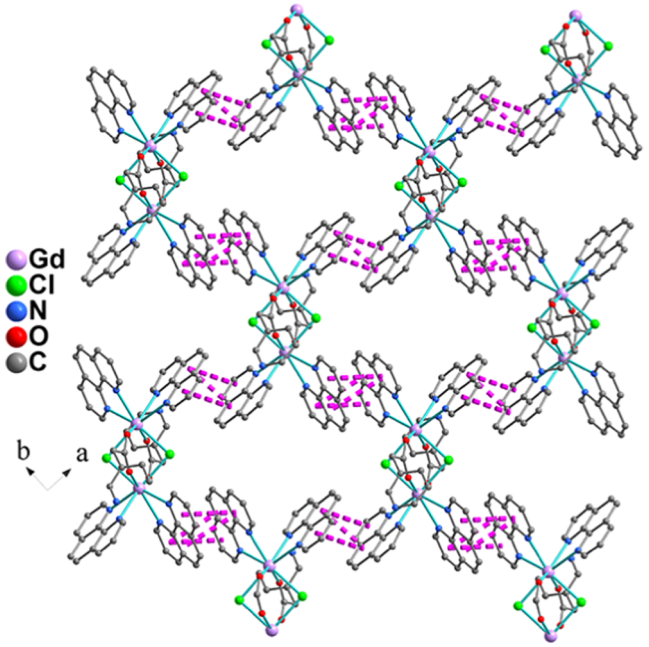

Figure 2. Two-dimensional supramolecular layer constructed by $\pi\cdots\pi$ interactions (pink dashed lines) in **1** along the *ab* plane.

studies showed that those spin centers bearing large spin, single-ion isotropy, and low-lying excited spin states such as Fe^{3+}, Mn^{2+}, and Gd^{3+} had great potential application in constructing high-performance materials.[46,47] In particular, compared with strong magnetic couplings existing in Fe^{3+} and Mn^{2+} compounds, weak magnetic interactions in Gd^{3+} compounds stemmed from the shielding of its 4f orbital improved magnetic refrigeration materials with large MCE. Thus, here, the magnetic properties and MCE of complex **1** were investigated. The plots of χ_M and $\chi_M T$ of **1** in a constant field of 1000 Oe in the temperature range of 2.0−300 K are illustrated in Figure 3a. χ_M displayed a gradual increase from

https://doi.org/10.1021/acsomega.1c04728
ACS Omega 2022, 7, 2604−2612

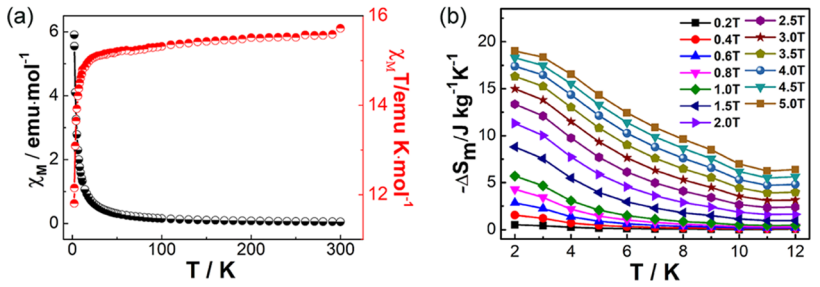

Figure 3. (a) Temperature dependence of the magnetic susceptibility for complex **1** between 2 and 300 K. (b) $-\Delta S_m$ for complex **1** calculated using the magnetization data at variable fields and temperatures.

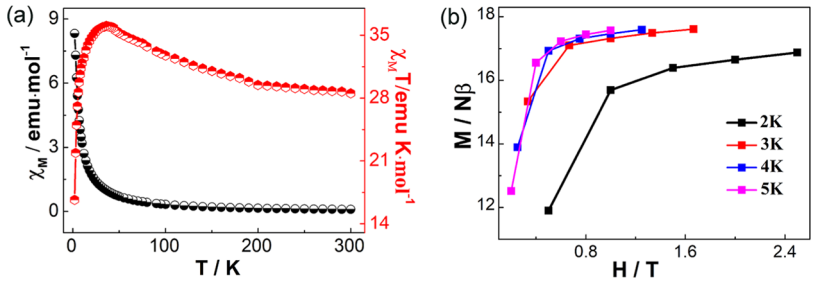

Figure 4. (a) Temperature dependence of the magnetic susceptibility for complex **2** between 2 and 300 K. (b) M vs H/T curves for complex **2**.

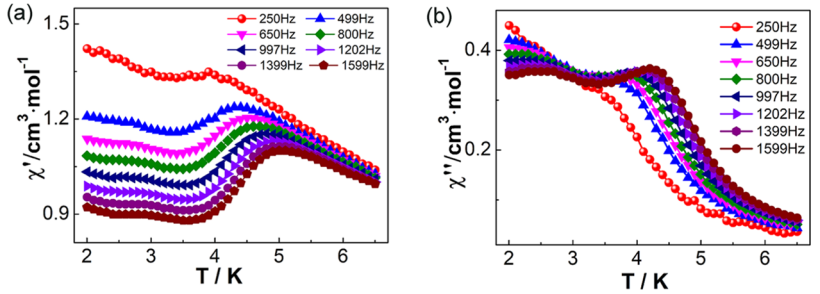

Figure 5. Plots of the temperature-dependent (a) in-phase (χ') and (b) out-of-phase (χ'') ac susceptibilities of complex **2** under a 2000 Oe dc field.

0.052 $cm^3\ mol^{-1}$ at 300 K to 0.54 $cm^3\ mol^{-1}$ at 28 K and then exponentially reached the maximum value of 5.87 $cm^3\ mol^{-1}$ at 2 K. Correspondingly, $\chi_M T$ of 15.61 $cm^3\ K\ mol^{-1}$ at 300 K for **1** was in good agreement with the theoretical value (15.75 $cm^3\ K\ mol^{-1}$) for two uncoupled Gd^{III} ($S = 7/2$, $L = 5$, $^8H_{7/2}$, $g = 2$) ions.[48] As the temperature decreased, χT increased gently and remained nearly constant and then sharply declined to the minimum value of 11.73 $cm^3\ K\ mol^{-1}$ at 2 K, which was related to the total zero-field splitting or the antiferromagnetic exchange interactions between two Gd^{III} cations. The $1/\chi-T$ plot of **1** followed the Curie–Weiss law with a negative Weiss constant $\theta = -1.14$ K in the temperature range of 2–300 K (Figure S4 in the SI), which further confirmed antiferromagnetic couplings among adjacent Gd^{III} ions. We studied the magnetic entropy changes $-\Delta S_m$ to investigate the MCE of the Gd_2 complex. Therefore, the magnetization measurements of **1** were measured in the range of 0–5 T at 2 K (Figure S5 in the SI), and the $M-H$ curves increased gradually with the increase of applied field. Moreover, M of **1** was 14.31 $N\beta$ at 2 K and 5 T, which was consistent with the expected value of 14.00 $N\beta$ for two isolated Gd^{III} ions ($g = 2.00$). The magnetic entropy change (ΔS_m^{max}), that is, a key parameter in evaluating the MCE, can be calculated on the basis of the Maxwell equation $\Delta S_m^{max} = \int [\partial M(T,H)/\partial T]_H \, dH$.[49,50] Based on the experimental magnetization data, ΔS_m values of **1** at variable temperatures and applied magnetic fields were obtained (Figure S6 in the SI). The largest $-\Delta S_m$ value was 19.03 J $kg^{-1}\ K^{-1}$ at 2 K under the condition $\Delta H = 5$ T (Figure 3b), which was slightly smaller than the theoretical value for two noninteracted Gd^{III} ions based on the equation $-\Delta S_m^{max} = nR\ln(2S_{Gd} + 1)/M_W$, in which n represents the number of Gd^{III} per mole, R is the gas constant, and S is the spin state. This phenomenon can be assigned to the presence of weak antiferromagnetic couplings among the Gd^{III} ions and a small metal/ligand mass ratio.[51] The magnetocaloric effect (MCE) of **1** (19.03 J $K^{-1}\ kg^{-1}$ at 2 K and 5 T) is compared to the reported complex $[Gd_4(acac)_4(\mu_2\text{-}OH)(L)_6]\cdot x CH_3CN\cdot y C_2H_5OH$ (Hacac = acetylacetone, HL = 5-(4-ethylbenzylidene)-8-hydroxylquinoline, 21.2 J $kg^{-1}\ K^{-1}$ at 2 K and 5 T).[52] Moreover, its MCE of 12.5 J $K^{-1}\ kg^{-1}$ at 2 K and 2 T is slightly lower than that of commercial $Gd_3Ga_5O_{12}$ (14.6 J $kg^{-1}\ K^{-1}$ at 2 K and 2 T)[53] but can be comparable to that of the reported $Gd_5BSi_2O_{13}$ (12.2 J $kg^{-1}\ K^{-1}$ at 2 K and 2 T).[54]

The direct-current (dc) magnetic susceptibility of **2** was also investigated in the temperature range of 1.8–300 K under 1000 Oe (Figure 4a). Upon reducing the temperature, the χ_M value of **2** slowly increased from 0.098 emu mol^{-1} at 300 K to 0.327 emu mol^{-1} at 100 K and then sharply reached the maximum value of 8.32 emu mol^{-1} at 2 K. The $\chi_M T$ value of **2** at 300 K was 28.08 $cm^3\ K\ mol^{-1}$, which was in good agreement

https://doi.org/10.1021/acsomega.1c04728
ACS Omega 2022, 7, 2604–2612

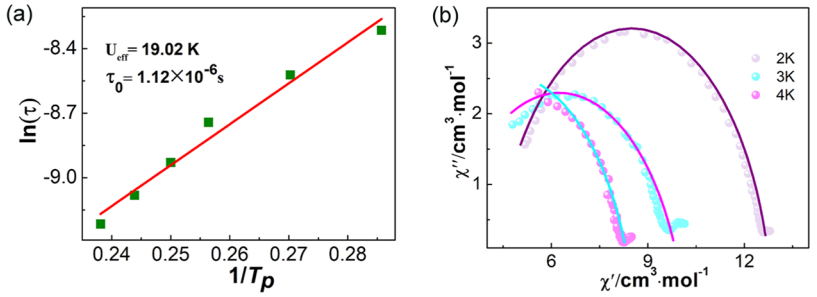

Figure 6. (a) Magnetization relaxation time ln τ vs T^{-1} plots for **2** under a dc field of 2000 Oe (the red solid line is fitted with the Arrhenius law). (b) Cole−Cole plots of **2** measured at 2, 3, and 4 K with a 2000 Oe dc field (the solid line represents the least-squares fitting using CC-FIT software).

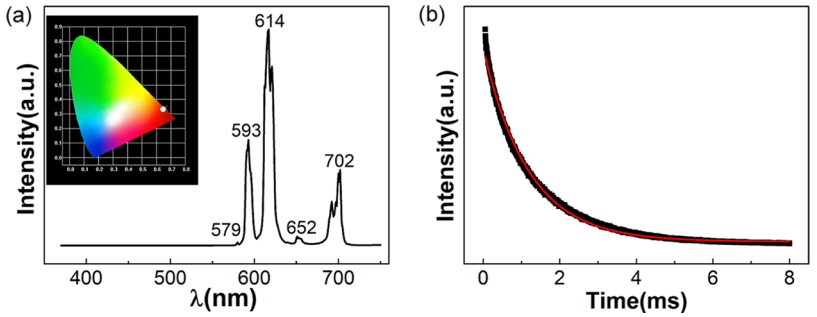

Figure 7. (a) Soild-state emission spectra for **3** at room temperature; the inset is the Commission internationale de l'éclairage (CIE) plot of **3**. (b) Decay curves of the Eu^{III} ($^5D_0 \rightarrow {}^7F_2$) complex **3**.

with the expected value of 28.34 cm^3 K mol^{-1} for two isolated Dy^{III} ions (S = 5/2, L = 5, $^6H_{15/2}$, g = 4/3). Upon cooling, a gradual increase in $\chi_M T$ was observed for **2**, reaching the maximum value of 35.75 cm^3 K mol^{-1} at 36 K, and then $\chi_M T$ decreased rapidly below this temperature, reaching the maximum value of 16.55 cm^3 K mol^{-1} at 2 K. This phenomenon is the result of the combination of the depopulation of M_j levels of the Dy(III) ion and the ferromagnetic interaction between the Dy(III) ions.[55−58] The field dependence of the magnetization of **2** was examined at 2−5 K (Figure 4b). The magnetization of 16.8 $N\beta$ at 50 kOe and 2 K was smaller than the theoretical saturation value of 20 $N\beta$ (10 $N\beta$ for each Dy^{III} ion). Moreover, M vs H/T curves displayed a nonsuperimposable nature. These phenomena indicated the presence of strong magnetic anisotropy associated with **2**.[59]

The frequency dependence of ac susceptibilities was tested to study the magnetic properties of **2**. As shown in Figure S7 in SI, no out-of-phase signal (χ'') appeared for the high frequency of 997 Hz at H_{ac} = 2.50 Oe and H_{dc} = 0 Oe in the temperature range of 1.8−15 K. When a dc field of 2000 Oe was applied, QTM was evidently suppressed. As shown in Figure 5, both in-phase (χ') and out-of-phase (χ'') curves showed a clear frequency dependence, which suggested the SMM behavior of **2**.[60] In addition, the Cole−Cole plots of **2** between 2 and 4 K displayed one characteristic magnetic relaxation (Figures 6b and S8), and the breadth of the distribution of relaxation was analyzed using a generalized Debye model (Table S3 in the SI). These α values (0.186−0.258) were not small, indicating that **2** had a relatively wide distribution of relaxation time. Moreover, the Debye model based on the relationship $\ln(\chi''/\chi') = \ln(\omega\tau_0) + E_a/K_{BT}$ was used to fit the frequency-dependent ac susceptibility data in the range of 650−1599 Hz (Figure 6a), and the energy barrier of 19.02 K and τ_0 value of 1.12×10^{-6} s for **2** were obtained, which were consistent with the expected numbers ($\tau_0 = 10^{-6}$−10^{-11} s) for SMMs. The U_{eff}/k value of **2** was consistent with that of carboxylic-based Dy^{III}-SMMs $[Dy_2(L)_3(H_2O)_3]\cdot$DMF (U_{eff} = 24.57K; H_2L = 3-(3,5-dicarboxylphenoxy)pyridine).[61]

Photoluminescent Properties. Ln-based complexes displayed unique and excellent photoluminescent properties, which were caused by the internal electron transitions in the 4f shell of Ln ions.[62,63] Thus, the luminescent properties of Ln-based complexes have attracted considerable attention because of their wide applications in sensors, light-emitting diodes, optical switches, displays, and functional probes in biological systems.[64,65] Herein, the photoluminescent properties of complexes **3** and **4** have been studied in solid state at room temperature.

As shown in Figure 7a, upon the excitation at 349 nm (Figure S9 in the SI), the emission spectra of **3** in the visible region exhibited five emission peaks at $^5D_0 \rightarrow {}^7F_0$ (579 nm), $^5D_0 \rightarrow {}^7F_1$ (593 nm), $^5D_0 \rightarrow {}^7F_2$ (614 nm), $^5D_0 \rightarrow {}^7F_5$ (653 nm), and $^5D_0 \rightarrow {}^7F_4$ (702 nm) with the characteristic transitions of the Eu^{III} ion.[66−68] The literature shows that the $^5D_0 \rightarrow {}^7F_2$ transitions of the Eu(III) cation were electric dipole transitions being hypersensitive to their local environments, whereas its $^5D_0 \rightarrow {}^7F_1$ transitions were magnetic dipole transitions being insensitive to the local environment.[69−71] Thus, the intensity ratio of I ($^5D_0 \rightarrow {}^7F_2$) and I ($^5D_0 \rightarrow {}^7F_1$) was often used as a probe to determine the site symmetry of a Eu(III) ion. In **3**, the value of I ($^5D_0 \rightarrow {}^7F_2$):I ($^5D_0 \rightarrow {}^7F_1$) was 1.6, indicating that the Eu(III) ion was located on the low-symmetry ligand field. This result was in good agreement with the above-mentioned single-crystal X-ray results, in which the Eu(III) ion of **3** had low-symmetry coordination configuration with a distorted square antiprism. Fluorescence lifetime was measured by monitoring the excitation at 349 nm and emission

https://doi.org/10.1021/acsomega.1c04728
ACS Omega 2022, 7, 2604−2612

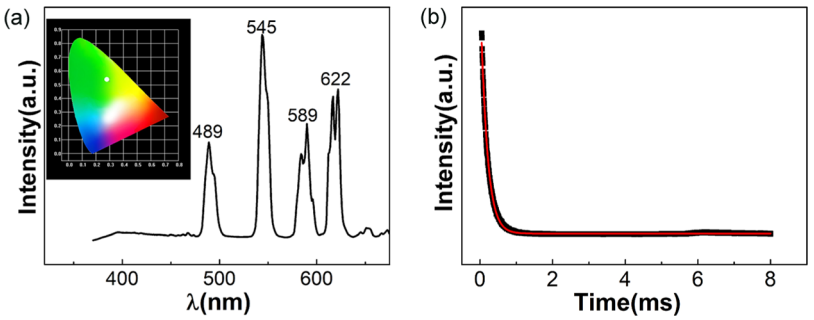

Figure 8. (a) Soild-state emission spectra for **4** at room temperature; the inset is the CIE plot of **4**. (b) Decay curves of the Tb^{III} ($^5D_4 \rightarrow {}^7F_5$) complex **4**.

at 614 nm to study the fluorescence behavior of **3** (Figure 7b). The decay curve of **3** can be fitted well by a monoexponential function $I = I_0 \exp(-t/\tau)$,[72,73] leading to the luminescence lifetime τ of 1.49 ms. This lifetime value was consistent with those reported of the Eu^{III} complex based on pyridinecarboxylic ligands.[74]

As for **4**, the characteristic emission spectra in the visible region were obtained upon excitation at 349 nm (Figure S10 in the SI), and they revealed four groups of characteristic single bands at 489, 545, 589, and 622 nm (Figure 8a), which can be assigned to $^5D_4 \rightarrow {}^7F_6$, $^5D_4 \rightarrow {}^7F_5$, $^5D_4 \rightarrow {}^7F_4$, and $^5D_4 \rightarrow {}^7F_3$ electron transitions of the Tb^{III} ion, respectively. Moreover, the fluorescence lifetime of **4** in the visible region was examined using the strongest emission (545 nm) and excitation (349 nm) with the decay curve (Figure 8b). The decay behavior followed the double-exponential function $I = A_1 \exp(-t/\tau_1) + A_2 \exp(-t/\tau_2)$, leading to the lifetime value of approximately 0.20 ms, which was in comparison with those reported for Tb^{III} complexes.[75]

Furthermore, the chromaticity coordinates for **3** and **4** based on the visible fluorescence spectrum are shown in the CIE 1931 diagram, which can reflect the specific emission color of the complexes. As shown in the insets of Figures 7a and 8a, the CIE chromaticity coordinates (X, Y) for **3** and **4** were (0.6512, 0.3433) and (0.2871, 0.5361), corresponding to the intense red and green emission of Eu^{III} and Tb^{III} ions, respectively. Therefore, the systematic study on the luminescence properties of these Eu^{III} and Tb^{III} species showed that they had strong emissions and long lifetime, indicating that the photoenergy transfer from the PAA^{1-} and phen linker excited state to the excited state of Eu^{III}/Tb^{III} was efficient.

CONCLUSIONS

Four lanthanide (Gd^{III}, Dy^{III}, Eu^{III}, and Tb^{III}) coordination molecules featuring dinuclear structures were prepared using 3-pyridylacetic acid ligand and the simplest *N,N′* bulky (1,10-phenanthroline) as the auxiliary ligand. In particular, the four complexes were the first lanthanide-based complexes constructed from 3-PAA. The magnet studies showed that the Gd^{III} derivative possessed MCE, and the Dy^{III} derivative displayed a typical SMM behavior. Moreover, the Eu^{III} and Tb^{III} derivatives displayed strong characteristic emission and long lifetime, indicating that the ligands were good luminescent sensitizers to Eu^{III} and Tb^{III} ions. Thus, the four complexes might be a good candidates in the molecular luminescent/magnet fields.

EXPERIMENTAL SECTION

Materials and Instruments. 3-Pyridylacetic acid, 1,10-phenanthroline, and $Ln(ClO_4)_3 \cdot 6H_2O$ were used as purchased without further purification. Fourier transform infrared (FT-IR) spectra were recorded using a PerkinElmer Spectrum One Spectrometer in the range of 4000−400 cm^{-1} using KBr pellets as bases. Element analyses of C, H, and N were conducted using an Elementar Vario EL III microanalyzer. Powder X-ray diffraction (PXRD) patterns at room temperature were collected on a Rigaku Miniflex II diffractometer using Mo Kα radiation (λ = 1.540598 Å). Simulated PXRD patterns were obtained from Mercury version 1.4 software (http://www.ccdc.cam.ac.uk/products/mercury). TGA measurements have been performed on polycrystalline samples under air atmosphere with a heating rate of 10 °C min^{-1} in the temperature range of 25−800 °C. Magnetic susceptibilities were performed on a Quantum Design PPMS model 6000 magnetometer. Photoluminescence analyses were conducted using an Edinburgh FL S920 fluorescence spectrometer.

Preparations of $[Ln_2(3\text{-}PAA)_2(\mu\text{-}Cl)_2(phen)_4](ClO_4)_2$ [Ln = Gd(1), Dy(2), Eu(3), Tb(4)]. A mixture of $Ln(ClO_4)_3 \cdot 6H_2O$ (0.5 mmol), 3-PAA·HCl (0.5 mmol), phen (0.5 mmol), Et_3N (0.20 mL), and CH_3CN (10 mL) with a starting pH of 6 was sealed into a 25 mL Teflon-lined stainless steel container under autogenous pressure, kept at 170 °C for 2 days, and then cooled to room temperature at a rate of 6.4 °C h^{-1}. Sheet single crystals were filtered off from the solution, then washed with CH_3CN, and dried in air. Yield: 25% (based on Gd) for **1**. Yield: 22% (based on Dy) for **2**. Yield: 27% (based on Eu) for **3**. Yield: 28% (based on Tb) for **4**. IR (KBr, cm^{-1}) for Gd**1**: 623m, 725s, 851s, 933w, 1090vs, 1300w, 1394s, 1423s, 1515m, 1571vs, 1623s, 3075w, 3405w, 3849w; for Dy**2**: 621m, 725s, 848s, 933w, 1089vs, 1299w, 1394s, 1423s, 1515m, 1568vs, 1623s, 3080w, 3431w, 3849w; for Eu**3**: 623m, 725s, 849s, 932w, 1088vs, 1294w, 1391s, 1423s, 1513m, 1569s, 1618s, 3057w, 3359w, 3849w. for Tb**4**: 623m, 725s, 852s, 936w, 1088vs, 1298w, 1384s, 1423s, 1513m, 1575s, 1613s, 3071w, 3361w, 3849w. Anal. calcd for **1**: C, 47.21; H, 2.81; N, 8.88. Found: C, 46.8; H, 2.92; N, 9.09. Anal. calcd for **2**: C, 46.90; H, 2.79; N, 8.82. Found: C, 46.12; H, 2.89; N, 9.07. Anal. calcd for **3**: C, 47.53; H, 2.83; N, 8.94. Found: C, 47.01; H, 2.93; N, 9.13. Anal. calcd for **4**: C, 47.11; H, 2.80; N, 8.86. Found: C, 46.43; H, 2.92; N, 9.08. In the IR spectra of 3-pyridylacetic and 1,10-phenanthroline, and complexes **1**−**4**, the absorption bands at 1400−1600 cm^{-1} represent the skeletal vibrations of the pyridyl rings, and the broad band at ca. 3300−3450 cm^{-1} suggests that the O−H stretching of the carboxylic group.

https://doi.org/10.1021/acsomega.1c04728
ACS Omega 2022, 7, 2604−2612

Single-Crystal XRD Structure Determination. Single crystals were mounted on a Bruker SMART APEX CCD diffractometer using graphite-monochromated Mo Kα radiation (=0.71073 Å) at 293 K for complexes **1**−**4**. The structures were solved by direct methods using the Siemens SHELXTL version 5 package[76] and refined by full-matrix least-squares techniques. All nonhydrogen atoms were refined anisotropically. Nonhydrogen atoms were located by difference Fourier maps and subjected to anisotropic refinement. No higher space groups for **1**−**4** were found using the Platon software from the IUCr website (http://www.iucr.org/). The crystallographic data of **1**−**4** in CIF format were deposited in the Cambridge Crystallographic Data Center (CCDC nos. 2101132, 2101133, 2101134, and 2101135).

■ ASSOCIATED CONTENT

Supporting Information

The Supporting Information is available free of charge at https://pubs.acs.org/doi/10.1021/acsomega.1c04728.

Selected bond lengths (Å) for **1**−**4**; powder X-ray diffraction patterns of **1**−**4**; summary of SHAPE analysis for **1**; $[ClO_4]^-$ lying between the layers along the *a* axis in **1**; TGA plot of **1**; magnetic data of **1** and **2**; solid-state excitation spectra at room temperature for **3** and **4**; and IR spectra for **1**−**4** (PDF)

Crystallographic data file of **1** (CIF)

Crystallographic data file of **2** (CIF)

Crystallographic data file of **3** (CIF)

Crystallographic data file of **4** (CIF)

■ AUTHOR INFORMATION

Corresponding Authors

Ying-Bing Lu − *College of Chemistry and Chemical Engineering, Gannan Normal University, Ganzhou 341000, P. R. China; National-Local Joint Engineering Research Center of Heavy Metals Pollutants Control and Resource Utilization, Nanchang Hangkong University, Nanchang 330000, P. R. China;* orcid.org/0000-0002-9556-7071; Email: ybluhm@163.com

Shui-Dong Zhu − *College of Chemistry and Chemical Engineering, Gannan Normal University, Ganzhou 341000, P. R. China*; Email: zsd2002@sina.com

Cai-Ming Liu − *Beijing National Laboratory for Molecular Sciences, CAS Key Laboratory of Organic Solids, Institute of Chemistry, Chinese Academy of Sciences, Beijing 100190, P. R. China;* orcid.org/0000-0001-7184-6693; Email: cmliu@iccas.ac.cn

Authors

Jun-Wei Wu − *College of Chemistry and Chemical Engineering, Gannan Normal University, Ganzhou 341000, P. R. China*

Sheng-Qian Wang − *College of Chemistry and Chemical Engineering, Gannan Normal University, Ganzhou 341000, P. R. China*

Shi-Yong Zhang − *College of Chemistry and Chemical Engineering, Gannan Normal University, Ganzhou 341000, P. R. China*

Rong Li − *School of Materials Science & Engineering, Hubei University, Wuhan 430062, P. R. China*

Juan Li − *College of Chemistry and Chemical Engineering, Gannan Normal University, Ganzhou 341000, P. R. China*

Jia-Hao Ai − *College of Chemistry and Chemical Engineering, Gannan Normal University, Ganzhou 341000, P. R. China*

Yong-Rong Xie − *College of Chemistry and Chemical Engineering, Gannan Normal University, Ganzhou 341000, P. R. China*

Complete contact information is available at: https://pubs.acs.org/10.1021/acsomega.1c04728

Notes

The authors declare no competing financial interest.

■ ACKNOWLEDGMENTS

The authors gratefully acknowledge financial support by the NSF of China (21661005, 21871274, 22161002 and 21801071) and the Key Laboratory of Jiangxi University for Function of Materials Chemistry.

■ REFERENCES

(1) Long, J.; Guari, Y.; Ferreira, R. A. S.; Carlos, L. D.; Larionova, J. Recent advances in luminescent lanthanide based Single-Molecule Magnets. *Coord. Chem. Rev.* **2018**, *363*, 57−70.

(2) Xin, Y.; Wang, J. H.; Zychowicz, M.; Zakrzewski, J. J.; Nakabayashi, K.; Sieklucka, B.; Chorazy, S.; Ohkoshi, S. Dehydration−Hydration Switching of Single-Molecule Magnet Behavior and Visible Photoluminescence in a Cyanido-Bridged $Dy^{III}Co^{III}$ Framework. *J. Am. Chem. Soc.* **2019**, *141*, 18211−18220.

(3) Ma, Y. J.; Hu, J. X.; Han, S. D.; Pan, J.; Li, J. H.; Wang, G. M. Manipulating On/Off Single-Molecule Magnet Behavior in a Dy(III)-Based Photochromic Complex. *J. Am. Chem. Soc.* **2020**, *142*, 2682−2689.

(4) Bernot, K.; Daiguebonne, C.; Calvez, G.; Suffren, Y.; Guillou, O. A Journey in Lanthanide Coordination Chemistry: From Evaporable Dimers to Magnetic Materials and Luminescent Devices. *Acc. Chem. Res.* **2021**, *54*, 427−440.

(5) Zheng, X. Y.; Jiang, Y. H.; Zhuang, G. L.; Liu, D. P.; Liao, H. G.; Kong, X. J.; Long, L. S.; Zheng, L. S. A Gigantic Molecular Wheel of $\{Gd_{140}\}$: A New Member of the Molecular Wheel Family. *J. Am. Chem. Soc.* **2017**, *139*, 18178−18181.

(6) Zhu, Z. H.; Guo, M.; Li, X. Y.; Tang, J. K. Molecular magnetism of lanthanide: Advances and perspectives. *Coord. Chem. Rev.* **2019**, *378*, 350−364.

(7) Chen, W. P.; Liao, P. Q.; Yu, Y.; Zheng, Z.; Chen, X. M.; Zheng, Y. Z. A Mixed-Ligand Approach for a Gigantic and Hollow Heterometallic Cage $\{Ni_{64}RE_{96}\}$ for Gas Separation and Magnetic Cooling Applications. *Angew. Chem., Int. Ed.* **2016**, *55*, 9375−9379.

(8) Cui, C.; Ju, W.; Luo, X.; Lin, Q.; Cao, J.; Xu, Y. A Series of Lanthanide Compounds Constructed from Ln_8 Rings Exhibiting Large Magnetocaloric Effect and Interesting Luminescence. *Inorg. Chem.* **2018**, *57*, 8608−8614.

(9) Li, J. H.; Liu, A. J.; Ma, Y. J.; Han, S. D.; Hu, J. X.; Wang, G. M. A large magnetocaloric effect in two hybrid Gd-complexes: the synergy of inorganic and organic ligands towards excellent cryomagnetic coolants. *J. Mater. Chem. C* **2019**, *7*, 6352−6358.

(10) Liu, C. M.; Zhang, D. Q.; Xiong, R. G.; Hao, X.; Zhu, D. B. A homochiral Zn−Dy heterometallic left-handed helical chain complex without chiral ligands: anion-induced assembly and multifunctional integration. *Chem. Commun.* **2018**, *54*, 13379−13382.

(11) Taguchi, Y.; Sakai, H.; Choudhury, D. Magnetocaloric Materials with Multiple Instabilities. *Adv. Mater.* **2017**, *29*, No. 1606144.

(12) Gil, Y.; Fuentealba, P.; Vega, A.; Spodine, E.; Aravena, D. Control of Magnetic Anisotropy by Macrocyclic Ligand Distortion in a Family of Dy^{III} and Er^{III} Single Molecule Magnets. *Dalton Trans.* **2020**, *49*, 17709−17718.

(13) DaCunha, T. T.; Jung, J.; Boulon, M. E.; Campo, G.; Pointillart, F.; Pereira, C. L. M.; LeGuennic, B.; Cador, O.; Bernot, K.; Pineider, F.; Golhen, S.; Ouahab, L. Magnetic Poles Determinations and

Robustness of Memory Effect upon Solubilization in a Dy^{III}-Based Single Ion Magnet. *J. Am. Chem. Soc.* **2013**, *135*, 16332−16335.
(14) Hilgar, J. D.; Bernbeck, M. G.; Rinehart, J. D. Million-fold Relaxation Time Enhancement across a Series of Phosphino-Supported Erbium Single-Molecule Magnets. *J. Am. Chem. Soc.* **2019**, *141*, 1913−1917.
(15) Li, R. P.; Liu, Q. Y.; Wang, Y. L.; Liu, C. M.; Liu, S. J. Evolution from linear tetranuclear clusters into one-dimensional chains of Dy(III) single-molecule magnets with an enhanced energy barrier. *Inorg. Chem. Front.* **2017**, *4*, 1149−1156.
(16) Kalita, P.; Nayak, P.; Ahmed, N.; Herrera, J. M.; Venkatasubbaiah, K.; Colacio, E.; Chandrasekhar, V. Seven-coordinate Ln^{III} complexes assembled from a bulky (Mes)acacH ligand: their synthesis, structure, photoluminescence and SMM behavior. *Dalton Trans.* **2020**, *49*, 15404−15416.
(17) Gonzalez, J. F.; Pointillart, F.; Cador, O. Hyperfine coupling and slow magnetic relaxation in isotopically enriched Dy^{III} mononuclear single- molecule magnets. *Inorg. Chem. Front.* **2019**, *6*, 1081−1086.
(18) Alexandropoulos, D. I.; Schulte, K. A.; Vignesh, K. R.; Dunbar, K. R. Slow magnetic dynamics in a family of mononuclear lanthanide complexes exhibiting the rare cubic coordination geometry. *Chem. Commun.* **2018**, *54*, 10136−10139.
(19) Guo, M.; Zhang, Y. Q.; Zhu, Z. H.; Tang, J. K. Dysprosium Compounds with Hula-Hoop-like Geometries: The Influence of Magnetic Anisotropy and Magnetic Interactions on Magnetic Relaxation. *Inorg. Chem.* **2018**, *57*, 12213−12221.
(20) Zhang, K.; Li, G. P.; Zhang, C.; Wang, Y. Y. Dramatic impact of auxiliary ligands on the two-step magnetic relaxation process in Dy_4^{III} single-molecule magnets. *Dalton Trans.* **2019**, *48*, 5793−5799.
(21) Goodwin, C. A. P.; Ortu, F.; Reta, D.; Chilton, N. F.; Mills, D. P. Molecular magnetic hysteresis at 60 kelvin in dysprosocenium. *Nature* **2017**, *548*, 439−442.
(22) Guo, F. S.; Day, B. M.; Chen, Y. C.; Tong, M. L.; Mansikkamakiand, A.; Layfield, R. A. Magnetic hysteresis up to 80 kelvin in a dysprosium metallocene single-molecule magnet. *Science* **2018**, *362*, 1400−1403.
(23) Xin, Y.; Wang, J. H.; Zychowicz, M.; Zakrzewski, J. J.; Nakabayashi, K.; Sieklucka, B.; Chorazy, S.; Ohkoshi, S. Dehydration−Hydration Switching of Single-Molecule Magnet Behavior and Visible Photoluminescence in a Cyanido-Bridged $Dy^{III}Co^{III}$ Framework. *J. Am. Chem. Soc.* **2019**, *141*, 18211−18220.
(24) Zhang, P.; Guo, Y. N.; Tang, J. K. Recent advances in dysprosium-based single molecule magnets: Structural overview and synthetic strategies. *Coord. Chem. Rev.* **2013**, *257*, 1728−1763.
(25) Li, L.; Zhu, Y. L.; Zhou, X. H.; Brites, C. D. S.; Ananias, D.; Lin, Z.; Paz, F. A. A.; Rocha, J.; Huang, W.; Carlos, L. D. Visible-Light Excited Luminescent Thermometer Based on Single Lanthanide Organic Frameworks. *Adv. Funct. Mater.* **2016**, *26*, 8677−8684.
(26) Zhou, X.; Wang, H. W.; Jiang, S.; Xiang, G. T.; Tang, X.; Luo, X. B.; Li, L.; Zhou, X. J. Multifunctional Luminescent Material Eu(III) and Tb(III) Complexes with Pyridine-3,5-Dicarboxylic Acid Linker: Crystal Structures, Tunable Emission, Energy Transfer, and Temperature Sensing. *Inorg. Chem.* **2019**, *58*, 3780−3788.
(27) Li, P.; Li, H. R. Recent progress in the lanthanide-complexes based luminescent hybrid materials. *Coord. Chem. Rev.* **2021**, *441*, No. 213988.
(28) Ayscue, R. L.; Verwiel, C. P.; Bertke, J. A.; Knope, K. E. Excitation-Dependent Photoluminescence Color Tuning in Lanthanide-Organic Hybrid Materials. *Inorg. Chem.* **2020**, *59*, 7539−7552.
(29) Ritchie, C.; Moore, E. G.; Speldrich, M.; Kögerler, P.; Boskovic, C. Terbium Polyoxometalate Organic Complexes: Correlation of Structure with Luminescence Properties. *Angew. Chem., Int. Ed.* **2010**, *49*, 7702−7705.
(30) Comby, S.; Tuck, S. A.; Truman, L. K.; Kotova, O.; Gunnlaugsson, T. New Trick for an Old Ligand! The Sensing of Zn(II) Using a Lanthanide Based Ternary Yb(III)-cyclen-8-hydroxyquinoline System As a Dual Emissive Probe for Displacement Assay. *Inorg. Chem.* **2012**, *51*, 10158−10168.
(31) Casanovas, B.; Speed, S.; Fallah, M. S. E.; Vicente, R.; Bardía, M. F.; Zinna, F.; Bari, L. D. Chiral dinuclear Ln(III) complexes derived from S- and R-2-(6-methoxy-2-naphthyl)propionate. Optical and magnetic properties. *Dalton Trans.* **2019**, *48*, 2059−2067.
(32) Bommakanti, S.; Venkataramudu, U.; Das, S. K. Functional Coordination Polymers from a Bifunctional Ligand: A Quantitative Transmetalation via Single Crystal to Single Crystal Transformation. *Cryst. Growth Des.* **2019**, *19*, 1155−1166.
(33) Teo, P.; Koh, L. L.; Hor, T. S. A. Na^+ and Ca^{2+} ion selective pyridylcarboxylate rings of Pd(II) and Pt(II). *Dalton Trans.* **2009**, *29*, 5637−5646.
(34) Wang, L.; Yin, X. H.; Hao, H. J.; Lin, W.; Tan, X. H.; Lin, C. W. Crystal structure of (E)-3-(3,4-dihydroxyphenyl)-N-methylacrylamide, $C_{10}H_{11}NO_3$. *Z. Kristallogr.—New Cryst. Struct.* **2011**, *226*, 219−220.
(35) Adams, C. J.; Crawford, P. C.; Guy Orpen, A.; Podesta, T. J. Cationand anion diversity in $[M(dithiooxalate)_2]^{2-}$ salts: structure robustness in crystal synthesis. *Dalton Trans.* **2006**, *34*, 4078−4092.
(36) Martin, D. P.; Springsteen, C. H.; LaDuca, R. L. Hydrothermal synthesis, structural determination, and thermal properties of 2-D cobalt- and nickel-based coordination polymers incorporating pendant-arm 3-pyridinecarboxylate ligands. *Inorg. Chim. Acta* **2007**, *360*, 599−606.
(37) Dong, L.; Lu, Y. B.; Zhu, S. D.; Wu, J. W.; Zhang, X. T.; Liao, Y.; Liu, C. M.; Liu, S. J.; Xie, Y. R.; Zhang, S. Y. A new family of dinuclear lanthanide complexes exhibiting luminescence, magnetic entropy changes and single molecule magnet behaviors. *CrystEngComm* **2021**, *23*, 645−652.
(38) Lu, Y. B.; Jiang, X. M.; Zhu, S. D.; Du, Z. Y.; Liu, C. M.; Xie, Y. R.; Liu, L. X. Anion Effects on Lanthanide(III) Tetrazole-1-acetate Dinuclear Complexes Showing Slow Magnetic Relaxation and Photofluorescent Emission. *Inorg. Chem.* **2016**, *55*, 3738−3749.
(39) Casanova, D.; Cirera, J.; Llunell, M.; Alemany, P.; Avnir, D.; Alvarez, S. Minimal distortion pathways in polyhedral rearrangements. *J. Am. Chem. Soc.* **2004**, *126*, 1755−1763.
(40) Rosenstengel, K.; Schulz, A.; Niehaus, O.; Janka, O.; Pottgen, R.; Villinger, A. Binary Polyazides Of Cerium And Gadolinium. *Eur. J. Inorg. Chem.* **2018**, *2018*, 778−790.
(41) Zhang, J. S.; Hao, Z. Q.; Gao, W.; Xin, L.; Zhang, L.; Mu, Y. Y, Lu, and Gd Complexes of NCO/NCS Pincer Ligands: Synthesis, Characterization, and Catalysis in the cis-1,4-Selective Polymerization of Isoprene. *Chem.—Asian J.* **2013**, *8*, 2079−2087.
(42) Lu, Y. B.; Jian, F. M.; Jin, S.; Zhao, J. W.; Xie, Y. R.; Luo, G. T. Three-Dimensional Extended Frameworks Constructed from Dinuclear Lanthanide(III) 1,4-Naphthalenedicarboxylate Units with Bis-(2,2′-biimidazole) Templates: Syntheses, Structures, and Magnetic and Luminescent Properties. *Cryst. Growth Des.* **2014**, *14*, 1684−1694.
(43) Zheng, Y.-Z.; Zhou, G.-J.; Zheng, Z.; Winpenny, R. E. P. Molecule-based magnetic coolers. *Chem. Soc. Rev.* **2014**, *43*, 1462−1475.
(44) Liu, J. L.; Chen, Y. C.; Guo, F. S.; Tong, M. L. Recent advances in the design of magnetic molecules for use as cryogenic magnetic coolants. *Coord. Chem. Rev.* **2014**, *281*, 26−49.
(45) Li, J. H.; Liu, A. J.; Ma, Y. J.; Han, S. D.; Hu, J. X.; Wang, G. M. A large magnetocaloric effect in two hybrid Gd-complexes: the synergy of inorganic and organic ligands towards excellent cryomagnetic coolants. *J. Mater. Chem. C* **2019**, *7*, 6352−6358.
(46) Chen, Y. C.; Guo, F. S.; Liu, J. L.; Leng, J. D.; Vrábel, P.; Orendáč, M.; Prokleška, J.; Sechovský, V.; Tong, M. L. Switching of the Magnetocaloric Effect of MnIIGlycolate by Water Molecules. *Chem.—Eur. J.* **2014**, *20*, 3029−3035.
(47) Wu, J. W.; Wang, X.; Tian, C. B.; Du, S. W. A new approach to fabricate the Mn(II)-based magnetic refrigerant through incorporation of a diamagnetic $[LiO_4]$ spacer. *Dalton Trans.* **2018**, *47*, 2143−2147.
(48) Kumar, M.; Wu, L. H.; Kariem, M.; Franconetti, A.; Sheikh, H. N.; Liu, S. J.; Sahoo, S. C.; Frontera, A. A Series of Lanthanide-Based Metal−Organic Frameworks Derived from Furan-2,5-dicarboxylate

https://doi.org/10.1021/acsomega.1c04728
ACS Omega 2022, 7, 2604−2612

and Glutarate: Structure-Corroborated Density Functional Theory Study, Magnetocaloric Effect, Slow Relaxation of Magnetization, and Luminescent Properties. *Inorg. Chem.* **2019**, *58*, 7760−7774.
(49) Lorusso, G.; Sharples, J. W.; Palacios, E.; Roubeau, O.; Brechin, E. K.; Sessoli, M.; Rossin, R. A.; Tuna, F.; McInnes, E. J. L.; Collison, D.; Evangelisti, M. A. DenseMetal−Organic Framework for Enhanced Magnetic Refrigeration. *Adv. Mater.* **2013**, *25*, 4653−4656.
(50) Han, S. D.; Miao, X. H.; Liu, S. J.; Bu, X. H. Magnetocaloric effect and slow magnetic relaxation in two dense (3,12)-connected lanthanide complexes. *Inorg. Chem. Front.* **2014**, *1*, 549−552.
(51) Yao, M. X.; Cai, L. Z.; Deng, X. W.; Zhang, W.; Liu, S. J.; Cai, X. M. Self-assembly of rare octanuclear quad(double-stranded) cluster helicates showing slow magnetic relaxation and the magnetocaloric effect. *New J. Chem.* **2018**, *42*, 17652−17658.
(52) Wang, W. M.; Zhang, L.; Li, X. Z.; He, L. Y.; Wang, X. X.; Shi, Y.; Wang, J.; Dong, J.; Wu, Z. L. Structures, fluorescence properties and magnetic properties of a series of rhombus-shaped Ln_4^{III} clusters: magnetocaloric effect and single-molecule-magnet behavior. *New J. Chem.* **2019**, *43*, 12941−12949.
(53) Daudin, B.; Lagnier, R.; Salce, B. Thermodynamic Properties of The Gadolinium Gallium Garnet, $Gd_3Ga_5O_{12}$ between 0.05 and 25 K. *J. Magn. Magn. Mater.* **1982**, *27*, 315−322.
(54) Tao, C.; Li, R. High-Performance Magnetic Refrigerant Featuring One-Dimensional Gd-O Chains and O-Gd_3 Triangles. *Chem.—Asian J.* **2018**, *13*, 2834−2837.
(55) Yin, D.-D.; Chen, Q.; Meng, Y.-S.; Sun, H.-L.; Zhang, Y.-Q.; Gao, S. Slow magnetic relaxation in a novel carboxylate/oxalate/hydroxyl bridged dysprosium layer. *Chem. Sci.* **2015**, *6*, 3095−3101.
(56) Chen, H.-M.; Wang, W.-M.; Li, X.-Q.; Chu, X.-Y.; Nie, Y.-Y.; Liu, Z.; Huang, S.-X.; Shen, H.-Y.; Cui, J.-Z.; Gao, H.-L. Luminescence and magnetocaloric effect of Ln_4 clusters (Ln = Eu, Gd, Tb, Er) bridged by CO_3^{2-} deriving from the spontaneous fixation of carbon dioxide in the atmosphere. *Inorg. Chem. Front.* **2018**, *5*, 394−402.
(57) Guo, Y.-N.; Xu, G.-F.; Wernsdorfer, W.; Ungur, L.; Guo, Y.; Tang, J.; Zhang, H.-J.; Chibotaru, L. F.; Powell, A. K. Strong Axiality and Ising Exchange Interaction Suppress Zero-Field Tunneling of Magnetization of an Asymmetric Dy_2 Single-Molecule Magnet. *J. Am. Chem. Soc.* **2011**, *133*, 11948−11951.
(58) Liu, C.-M.; Zhang, D.-Q.; Hao, X.; Zhu, D.-B. Assembly of chiral 3d-4f wheel-like cluster complexes with achiral ligands: singlemolecule magnet behaviour and magnetocaloric effect. *Inorg. Chem. Front.* **2020**, *7*, 3340−3351.
(59) Gass, I. A.; Moubaraki, B.; Langley, S. K.; Batten, S. R.; Murray, K. S. A $\pi-\pi$ 3D network of tetranuclear μ_2/μ_3-carbonato Dy(iii) bis-pyrazolylpyridine clusters showing single molecule magnetism features. *Chem. Commun.* **2012**, *48*, 2089−2091.
(60) Long, J.; Rouquette, J.; Thibaud, J. M.; Ferreira, R. A. S.; Carlos, L. D.; Donnadieu, B.; Vieru, V.; Chibotaru, L. F.; Konczewicz, L.; Haines, J.; Guari, Y.; Larionova, J. A. High-Temperature Molecular Ferroelectric Zn/Dy Complex Exhibiting Single-Ion-Magnet Behavior and Lanthanide Luminescence. *Angew. Chem., Int. Ed.* **2015**, *54*, 2236−2240.
(61) Gao, W.; Zhou, A.; Wei, H.; Wang, C.; Liu, J.; Zhang, X. Water-stable Ln^{III}-based coordination polymers displaying slow magnetic relaxation and luminescence sensing properties. *New. J. Chem.* **2020**, *44*, 6747−6759.
(62) Ananias, D.; Paz, F. A. A.; Yufit, D. S.; Carlos, L. D.; Rocha, J. Photoluminescent Thermometer Based on a Phase-Transition Lanthanide Silicate with Unusual Structural Disorder. *J. Am. Chem. Soc.* **2015**, *137*, 3051−3058.
(63) Xu, X.; Chen, Y. H.; Zhang, Y.; Liu, Y. F.; Chen, L. J.; Zhao, J. W. Rare-Earth and Antimony-Oxo Clusters Simultaneously Connecting Antimonotungstates Comprising Divacant and Tetravacant Keggin Fragments. *Inorg. Chem.* **2019**, *58*, 11636−11648.
(64) Martínez-Calvo, M.; Kotova, O.; Mobius, M. E.; Bell, A. P.; McCabe, T.; Boland, J. J.; Gunnlaugsson, T. Healable Luminescent Self-Assembly Supramolecular Metallogels Possessing Lanthanide (Eu/Tb) Dependent Rheological and Morphological Properties. *J. Am. Chem. Soc.* **2015**, *137*, 1983−1992.
(65) Trivedi, E. R.; Eliseeva, S. V.; Jankolovits, J.; Olmstead, M. M.; Petoud, S.; Pecoraro, V. L. Highly Emitting Near-Infrared Lanthanide "Encapsulated Sandwich" Metallacrown Complexes with Excitation Shifted Toward Lower Energy. *J. Am. Chem. Soc.* **2014**, *136*, 1526−1534.
(66) Zhou, X. J.; Li, S. Y.; Zhou, X.; Chen, L. N.; Wu, J.; Yu, T. L.; Li, L.; Jiang, S.; Tang, X.; Xiang, G. T.; Li, Y. H. Luminescent Properties and Ratiometric Optical Thermometry of $LnBDCF_4$ Compounds. *Spectrochim. Acta, Part A* **2020**, *224*, No. 117418.
(67) Zhou, X.; Wang, H. W.; Jiang, S.; Xiang, G. T.; Tang, X.; Luo, X. B.; Li, L.; Zhou, X. J. Multifunctional Luminescent Material Eu(III) and Tb(III) Complexes with Pyridine-3,5-Dicarboxylic Acid Linker: Crystal Structures, Tunable Emission, Energy Transfer, and Temperature Sensing. *Inorg. Chem.* **2019**, *58*, 3780−3788.
(68) Wang, D.; Li, Y. M.; Zhang, Y.; Xu, X.; Liu, Y.; Chen, L. J.; Zhao, J. W. Construction of Ln^{3+}-Substituted Arsenotungstates Modified by 2,5-Thiophenedicarboxylic Acid and Application in Selective Fluorescence Detection of Ba^{2+} in Aqueous Solution. *Inorg. Chem.* **2020**, *59*, 6839−6848.
(69) Xu, Q.; Li, L.; Liu, X.; Xu, R. Incorporation of Rare-Earth Complex $Eu(TTA)_4C_5H_5NC_{16}H_{33}$ into Surface-Modified Si−MCM_{41} and Its Photophysical Properties. *Chem. Mater.* **2002**, *14*, 549−555.
(70) Choppin, G. R.; Peterman, D. R. Applications of lanthanide luminescence spectroscopy to solution studies of coordination chemistry. *Coord. Chem. Rev.* **1998**, *174*, 283−299.
(71) Han, Q.; Liu, J. C.; Wen, Y.; Chen, L. J.; Zhao, J. W.; Yang, G. Y. Tellurotungstate-Based Organotin−Rare-Earth Heterometallic Hybrids with Four Organic Components. *Inorg. Chem.* **2017**, *56*, 7257−7269.
(72) Zmojda, J.; Kochanowicz, M.; Miluski, P.; Dorosz, J.; Pisarska, J.; Pisarski, W. A.; Dorosz, D. Investigation of up conversion luminescence in antimony-germanatedouble-clad two cores optical fiber co-doped with Yb^{3+}/Tm^{3+} and Yb^{3+}/Ho^{3+} ions. *J. Lumin.* **2016**, *170*, 795−800.
(73) Xu, X.; Meng, R. R.; Lu, C. T.; Mei, L.; Chen, L. J.; Zhao, J. W. Acetate-Decorated Tri-Ln(III)-Containing Antimonotungstates with a Tetrahedral $\{WO_4\}$ Group as a Structure-Directing Template and Their Luminescence Propertie. *Inorg. Chem.* **2020**, *59*, 3954−3963.
(74) Jiang, J.; Duan, J.; Liu, J.; Chen, L.; Zhao, J. Lanthanide-Incorporated Borotungstates Including Keggin-Type $[BW_{11}O_{39}]^{9-}$ Fragments and Their Luminescence Properties. *Cryst. Growth. Des.* **2020**, *20*, 362−369.
(75) Li, R. F.; Li, R. H.; Liu, X. F.; Chang, X. H.; Feng, X. Lanthanide complexes based on a conjugated pyridine carboxylate ligand: structures, luminescence and magnetic properties. *RSC Adv.* **2020**, *10*, 6192−6199.
(76) *SHELXTL Reference Manual*, version 5; Siemens Energy & Automation Inc.: Madison, WI, 1994.

https://doi.org/10.1021/acsomega.1c04728
ACS Omega 2022, 7, 2604−2612